NUCLEAR SCIENCE AND ENGINEERING · VOLUME 184 · 561–574 · DECEMBER 2016

Ranking the Importance of Nuclear Reactions for Activation and Transmutation Events

Wayne Arter,[a]* J. Guy Morgan,[b] Samuel D. Relton,[c] and Nicholas J. Higham[c]

[a]*CCFE, Culham Science Centre, Abingdon, Oxon OX14 3DB, United Kingdom*
[b]*Culham Electromagnetics Ltd., Culham Science Centre, Abingdon, Oxon OX14 3DB, United Kingdom*
[c]*The University of Manchester, School of Mathematics, Manchester M13 9PL, United Kingdom*

Received February 25, 2015
Accepted for Publication June 5, 2016
http://dx.doi.org/10.13182/NSE15-23

Abstract — *Pathways-reduced analysis is one of the techniques used by the* FISPACT*-II nuclear activation and transmutation software to study the sensitivity of the computed inventories to uncertainties in reaction cross sections. Although deciding which pathways are most important is very helpful in for example determining which nuclear data would benefit from further refinement, pathways-reduced analysis need not necessarily define the most critical reaction, since one reaction may contribute to several different pathways. This work examines three different techniques for ranking reactions in their order of importance in determining the final inventory, comparing the pathways-based metric (PBM), the direct method, and a method based on the Pearson correlation coefficient. Reasons why the PBM is to be preferred are presented.*

Keywords — *FISPACT-II, pathways-reduced analysis.*

Note — *Some figures may be in color only in the electronic version.*

I. INTRODUCTION

FISPACT-II is a software suite for the analysis of nuclear activation and transmutation events of all kinds.[1] The present work focuses on its use in sensitivity studies of nuclear inventory calculations; these employ the Bateman model for the evolution of the inventory of a target subject to irradiation by an imposed flux of projectile particles, always neutrons herein. In Ref. 2 it was established that the pathways-reduced approach[3,4] to such studies almost invariably gives very close agreement with Monte Carlo sensitivities computed using full Bateman, i.e., accounting for all nuclides and pathways. Pathways-reduced models are, following Eastwood and Morgan,[3] identified by a graph-based approach that determines the key reaction pathways determining the inventory at a given time and eliminates from consideration those nuclides that do not lie on this reduced set of pathways.

The pathways-reduced metric is a sensitivity method in the respect that it implicitly selects a set of the most important nuclide reactions. A wide range of other sensitivity methods has been used in the nuclear industry as shown by literature reviews by Helton et al.[5] and comparative reviews by Ionescu-Bujor and Cacuci[6] and Cacuci and Ionescu-Bujor.[7] Indeed, sensitivity analyses are available as part of nuclear industry software packages such as DAKOTA (Ref. 8) and SCALE (Ref. 9). General-purpose sensitivity software is also available, such as OpenCossan.[10]

A key input to most techniques considered herein is an estimate of the uncertainties in the reaction cross section. The determination of such uncertainties is a challenging subject in its own right; hence, it is important to examine techniques that can identify which reactions most require further examination. The present work represents a comparison of three different techniques that exploit the pathways-based reduction for the nuclear activation problem.

*E-mail: wayne.arter@ukaea.uk

FISPACT-II can access uncertainty data, typically the standard deviation, for the vast majority of reaction cross sections in the EASY-II database[11]; however, no information is currently passed concerning pure decay reactions. This reflects the fact that half-lives are often very accurately known. There are other reactions in the database for which a value of zero uncertainty is found, usually indicating that no information is available. There are thus difficulties in making the comparison, the implications of which are discussed in Sec. II.D.

To proceed further with this introduction, it is efficient to introduce the time evolution (rate or Bateman equation) for a nuclear inventory X:

$$\frac{dX}{dt} = \mathsf{A}X \ , \tag{1}$$

where X is the vector of nuclide numbers and A is the matrix of nuclear interaction coefficients for both induced reactions and spontaneous decays. Note that one coefficient A_{ij} of A may represent several different nuclear reactions since the equation involves an average over a spectrum of energies (of neutrons in the present work, although other elementary particles may be considered in general). Hence, the term "interaction" is used to cover all effects generating nuclide i as the child of parent j. It is worth noting that although i precedes j alphabetically, reactions throughout this work will—except for the A_{ij}—be described in parent-child order. In general, the coefficients A_{ij} may change with time as the incident neutron flux changes.

All the techniques for ranking the interactions A_{ij} are most easily understood in the context of a single constant irradiation in the time interval $(0, t_f)$, producing an inventory $X(t_f)$. Different aspects of the inventory, such as heat production or kerma, may be studied using FISPACT-II, but for illustrative purposes it is sufficient to consider only the total activity

$$Q = \sum_k \lambda_k X_k(t_f) \ , \tag{2}$$

where λ_k is the decay rate of the nuclide X_k; λ_k is zero for stable nuclides and $\lambda_k = \log_e 2/\tau_k$ for unstable ones, where τ_k is the half-life. Although attention focuses here on FISPACT-II, the Bateman approach is standard in that most packages with a claim to generality—not only DAKOTA and SCALE in the United States but also ANSWERS (Ref. 12) with FISPIN in the United Kingdom—include solvers for the problem. The pathways-based analysis technique studied here could in principle be implemented in any of these codes.

The three different ranking techniques are described in Sec. II. Apart from the use of pathways-based reduction, there is novelty in the calculation of the direct sensitivity in that the matrix Fréchet derivative (see the Appendix) is used in its computation rather than the more usual decoupled direct method (DDM) of Dunker.[13] The application of the techniques to the wide range of test cases first introduced in Ref. 2 is illustrated in Sec. III. Last, Sec. IV compares the utility of the different techniques.

II. SENSITIVITY MEASURES

II.A. Pathways-Based Metric

The pathways-based metric (PBM) is calculated quite simply from the output of the pathways-reduced approach, which includes a listing of each pathway and its percentage contribution to the active nuclide at its termination. For a given interaction A_{ij}, all the numbers of pathways N_p upon which it lies are identified, and the PBM is calculated as

$$S^{ij}_{\mathrm{PBM}} = \sum_{k=1}^{N_p} p_l \lambda_t X_t I_{kl} \ , \tag{3}$$

where p_l is the fractional contribution of pathway l to the number of atoms X_t (evaluated at time t_f) in the inventory with decay rate λ_t and the indicator matrix $I_{kl} = 1$ or 0 depending on whether or not a reaction contributing to the interaction lies on the pathway.

Figure 1 illustrates how the definition works in a simplified case where irradiation of an initial sample consisting of X_1 atoms of nuclide 1 and X_2 atoms of nuclide 2 produces an inventory containing numbers X_5 and X_6 of radioactive nuclides 5 and 6, respectively, with three important pathways. The first pathway contributes $p_1 X_5$ atoms of nuclide 5, and the third pathway contributes $p_3 X_5$ atoms of nuclide 5. (Supposing the other pathways are unimportant, $p_1 + p_3 \approx 1$ and $p_2 \approx 1$.) The sensitivity of the inventory to the reaction with coefficient A_{32} (large arrowheads in Fig. 1) is then

$$S^{32}_{\mathrm{PBM}} = p_1 \lambda_5 X_5 + p_2 \lambda_6 X_6 \ , \tag{4}$$

where λ_5 is the decay rate of nuclide 5, etc.

This technique required special modification to FISPACT-II for its implementation, which was facilitated by the object-oriented design of the Fortran-95 code. For the purposes of initial investigation, the loops that are identified by the graph-based approach used by FISPACT-II are ignored.

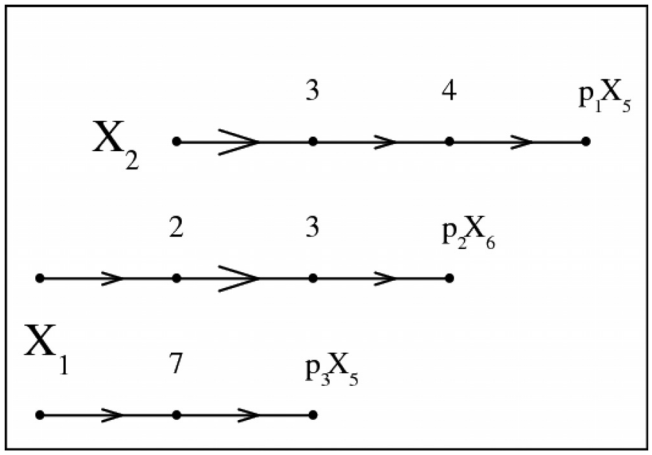

Fig. 1. Example illustrating how the PBM S_{PBM} is calculated when the three pathways shown are highlighted by the pathways-reduced analysis. The pathways are numbered in order 1, 2, and 3 from the top. Pathway 1 starts with nuclide 2 and generates via a sequence of reactions involving nuclides 3 and 4, p_1X_5 atoms of nuclide 5, whereas the other pathways begin with nuclide 1 and generate nuclides 6 and 5, respectively. The larger arrowheads indicate reactions with the coefficient of interest A_{32}.

II.B. Direct Method

The direct method (DM) works directly with the tensor describing the rate of variation of the nuclide X_k with respect to nuclear reaction coefficients. For initial investigative purposes, it is sufficient to consider the partial derivative with respect to A_{ij}. Differentiating Eq. (1) with (i, j) regarded as fixed gives

$$\frac{d}{dt}\left(\frac{\partial X}{\partial A_{ij}}\right) = A\frac{\partial X}{\partial A_{ij}} + \frac{\partial A}{\partial A_{ij}}X \ . \tag{5}$$

If the sensitivity of the total activity is required, then using Eq. (2), this is

$$S^{ij}_{\mathrm{DM}} = \sum_k \lambda_k \frac{\partial X_k(t_f)}{\partial A_{ij}} \ . \tag{6}$$

In the DDM, Eq. (5) is solved for $\partial X_k/\partial A_{ij}$ using a method that exploits the sparseness of $\partial A/\partial A_{ij} = \delta_{ij}$ in the present context. However, it is also possible to express S_{DM} in terms of the matrix Fréchet derivative as explained in the Appendix, namely,

$$S^{ij}_{\mathrm{FDM}}(t_f) = t_f \sum_k \lambda_k L_{\exp}(t_f \mathsf{A}, \mathsf{E}_{ij}) X(0) \ , \tag{7}$$

where $L_{\exp}$ is the matrix Fréchet derivative as defined in the Appendix where E_{ij} is also defined. Equation (7) defines the Fréchet direct method (FDM). Similarly to the PBM, this technique required modification of FISPACT-II to output the matrix A in a format suitable for input to MATLAB (Ref. 14).

II.C. Pearson Derived Method

The Pearson technique for ranking sensitivities starts with the definition of the Pearson product-moment correlation coefficient for a set of N_s samples $\{(A_s, Q_s) : s = 1, \ldots, N_s\}$, namely,

$$r = \frac{\sum_s (Q_s - \bar{Q})(A_s - \bar{A})}{(N_s - 1)\Delta Q \Delta A} \ , \tag{8}$$

where the suffix ij on r and A is to be understood, the overbar denotes average, and Δ denotes the standard deviation of the distribution so that for example

$$\bar{Q} = \frac{1}{N_s}\sum_{s=1}^{N_s} Q_s \tag{9}$$

and

$$\Delta Q = \sqrt{\frac{1}{(N_s - 1)}\sum_{s=1}^{N_s}[(Q_s)^2 - \bar{Q}^2]} \ . \tag{10}$$

The coefficient r_{ij} is by definition always ≤ 1, and a magnitude of r close to 1 indicates a strong linear correlation.

However, it is the proportionality constant corresponding to $\partial Q/\partial A_{ij}$ that is of initial interest. It is worth cautioning that although the definition implicitly implies a linear relation, there is no guarantee of this. However, in order to proceed, linearity will be assumed, namely,

$$Q - \bar{Q} = \tilde{r}(A - \bar{A}) \ , \tag{11}$$

and substituting in Eq. (8), it follows that

$$S_{\mathrm{PRD}} = \tilde{r}_{ij} = r_{ij}\left(\frac{\Delta Q}{\Delta A}\right) \ . \tag{12}$$

It follows that the output of the Monte Carlo sensitivity calculations may be used to rank the different interactions by computing $r_{ij}/\Delta A$ (note that ΔQ is the same for all the A_{ij} variations in the standard approach described in Ref. 2).

The calculation of the Pearson coefficient r is well known to be sensitive to round-off error. To avoid modifying the software, the coefficient is computed using output values from FISPACT-II given to only six significant

figures by default. This accuracy is the maximum that can be expected from the numerical integration of the rate equation that is constrained to an accuracy of one part in a million. It was found that splitting the separate contributions of A_s and $\bar{A}$ to Eq. (8) led to unacceptable cancellation due to round-off effects (although it was verified that round-off was not a similar issue for Q_s and $\bar{Q}$).

II.D. Comments upon the Different Metrics

The main distinction between the PBM and the other two measures is that the pathways-based method is global, capturing the whole variation of the inventory as parameters are varied, although having the disadvantage that it cannot measure sensitivity to diagonal entries of A. The other two techniques are more local; indeed, the DM returns directly only a coefficient at the mean of the distribution of Q. The Pearson method is somewhere in-between, using global variations but making a local linear assumption about the mean. This complicates the comparison in Sec. III.

The principal comment to be made concerning the comparison is that corresponding to the lack of sensitivity to element A_{ij} when it is zero due an absence of interaction between nuclides i and j, a large sensitivity in the local sense may be inconsequential for the total activity Q if the corresponding A_{ij} is relatively very small. However, the two more local estimates [Eqs. (6) and (12)] for $\partial Q/\partial A_{ij}$ should be directly comparable.

Main interest attaches to global measures such as S_{PBM}. The FDM approach may be used to produce an equivalent ranking by scaling by the estimated error in the coefficient, namely,

$$S^{ij}_{\mathrm{FDS}} = S^{ij}_{\mathrm{FDM}} \cdot \left(\frac{\epsilon_{ij}}{100}\right) \cdot \bar{A}_{ij} \ , \tag{13}$$

where ϵ_{ij} is the percentage error in the distribution of the coefficient A_{ij}. FISPACT-II returns both ϵ_{ij} and A_{ij} by combining the uncertainties in the reaction coefficients corresponding to A_{ij}.

From Eq. (12), a ranking based on the Pearson coefficient r should also be comparable to S_{PBM} if it is scaled similarly, namely,

$$S^{ij}_{\mathrm{PRS}} = r_{ij} \cdot \left(\frac{\epsilon_{ij}}{100}\right) \cdot \left(\frac{\bar{A}_{ij}}{\Delta A_{ij}}\right) \ . \tag{14}$$

In practice it is found that $S^{ij}_{\mathrm{PRS}} \approx r_{ij}$. The acronyms FDS and PRS will henceforth be used to denote scaled FDM and scaled Pearson method, respectively.

Note that for interactions for which no uncertainty information is available, neither can a Pearson coefficient be computed nor is S_{FDS} useful. The coefficient S_{PBM} may be nonzero, but this relies on the interaction's lying on a pathway important for other reasons. Interactions without accompanying uncertainty information will therefore largely have to be ignored in this work.

III. SENSITIVITY CALCULATIONS

III.A. Details of Cases

The test cases are taken from Ref. 2 and involve several different nuclide mixtures designed to be indicative of a wide range of activation problems; see Table I. As indicated, all but one of the mixtures consisted of 1 kg of material subject to a neutron flux of 10^{15} cm^{-2} · s^{-1} for a year, without any cooling period.

The mixtures are used in six test cases, with the Alloy case extended to include a cooling phase. Each test case is run using the full TENDL 2013 data from the EASY-II database[11] with pathways analysis to identify the important reactions, the numbers of which are listed in Table II.

TABLE I

Test Cases*

Test Label	Constituents of Mixture	Sample Mass	Irradiation Period	Cooling Period	Neutron Flux
Alloy	Fe 40.0 : Ni 20.0 : Cr 20.0 : Mn 20.0	1 kg	1 yr	0	10^{15} cm^{-2} · s^{-1}
Alloy+c	Fe 40.0 : Ni 20.0 : Cr 20.0 : Mn 20.0	1 kg	1 yr	1 yr	10^{15} cm^{-2} · s^{-1}
Fe	Fe	1 kg	2.5 yr	0	10^{15} cm^{-2} · s^{-1}
LiMix	Li 40.0 : Be 30.0 : O 30.0	1 kg	1 yr	0	10^{15} cm^{-2} · s^{-1}
WMix	W20.0 : Re 20.0 : Ir 20.0 : Bi 20.0 : Pb 20.0	1 kg	1 yr	0	10^{15} cm^{-2} · s^{-1}
Y2O3	Y 78.74 : O 21.20	1 g	300 s	0	1.116×10^{10} cm^{-2} · s^{-1}

*Each test case consists of numbers of atoms of the listed elements with their natural abundances of nuclides, given as percentages by mass of the whole.

TABLE II

Test Case Statistics*

Test Label	I, Reactions Examined	Matrix A Size	Maximum N_x, Samples per Reaction	N_s, Total Sample
Alloy	84	51	640	53760
Alloy+c	50	38	640	32000
Fe	27	24	640	17280
LiMix	17	21	640	10880
WMix	71	63	640	45440
Y2O3	13	16	2560	33280

*Monte Carlo sampling by FISPACT-II has a sample size determined by the number of reactions examined.

As in Ref. 2, Monte Carlo solution of the reduced problem, investigating the distributions of the important reaction rates specified in the newer database, was then performed in the sequence of increasing sample size per reaction, $N_x = 10, 40, 160, \ldots$ up to the maximum value specified in Table II. Indications from Ref. 2 and work that may be published elsewhere indicate that the pathways-reduced results agree to at least two (and often three) significant figures with those obtained by sampling the full problem, at less than a thousandth of the computational cost. As might be expected from the large maximum number of samples N_s employed, the distributions of reaction rates actually sampled usually agree in the mean to four significant figures with the nominal database values.

III.B. Results

This section presents results for each of the test cases in turn, in the alphabetic order specified in Table I. For each test case there is a table of sensitivity rankings ordered by Fréchet derivative amplitude and a graph of rankings ordered by S_{PBM}. The tables enable a larger range of interactions to be compared since the graphs become difficult to interpret once the number of plotted interactions exceeds about ten. Note the convention (except for the Y2O3 case) that all three methods must provide a ranking for the comparison to be plotted. So, in the following figures the ten highest-ranked cases plotted may include reactions significantly smaller in importance than the tenth.

A general feature of all graphs comparing rankings by the different techniques is the symmetry about the midline labeled "PBM." The appearance of "V" and "Λ" patterns indicates that although the more local measures may not agree with S_{PBM}, they do themselves correlate well.

For two of the test cases, Alloy+c in Sec. III.B.2 and WMix in Sec. III.B.5, further results of analysis are presented to help understand the effect of sampling and round-off on the calculation of S_{PRS}. In addition, a table of sensitivity rankings ordered by S_{PBM} and a graph of rankings ordered by the Fréchet derivative also appear in these two sections. (This information is omitted from Secs. III.B.1, III.B.3, III.B.4, and III.B.6 to save space.)

III.B.1. Alloy

See Table III and Fig. 2.

III.B.2. Alloy+c

See Tables IV, V, and VI and Figs. 3, 4, and 5.

Table IV suggests that once the Pearson correlation becomes below 0.1, it becomes inaccurate. Figure 3 shows that the smaller Pearson coefficients vary erratically with

TABLE III

Alloy Case: Rankings for Different Methods

Parent	Child	Sensitivity		
		FDS	PBM	PRS
Fe-56	Mn-56	1	5	1
Ni-58	Ni-57	21	37	57
Mn-55	Cr-55	10	11	10
Mn-55	V-52	12	18	12
Mn-55	Mn-56	9	1	9
Cr-52	Cr-51	17	19	24
Cr-52	V-52	5	10	5
Ni-58	Co-58*m*	3	4	3
Mn-55	Mn-54	11	6	11
Fe-56	Fe-55	14	15	15
Ni-58	Co-57	8	9	8
Ni-60	Co-60*m*	4	13	4
Ni-58	Co-58	2	2	2
Ni-58	Fe-55	7	12	6
Fe-54	Cr-51	13	20	13
Cr-53	V-52	37	0	0
Cr-53	V-53	15	25	18
Fe-54	Mn-54	6	8	7
Cr-50	Cr-51	22	3	30
Fe-57	Mn-56	36	0	0
Fe-57	Mn-57	18	26	33
Ni-62	Fe-59	19	35	71
Ni-62	Co-62*m*	30	50	56
Ni-62	Co-61	39	79	66
Ni-62	Co-62	28	46	47
Ni-60	Co-60	16	28	14
Cr-54	Cr-55	24	22	67
Cr-54	Ti-51	27	49	26
Cr-54	V-54	25	52	50
Fe-54	Fe-55	26	14	48

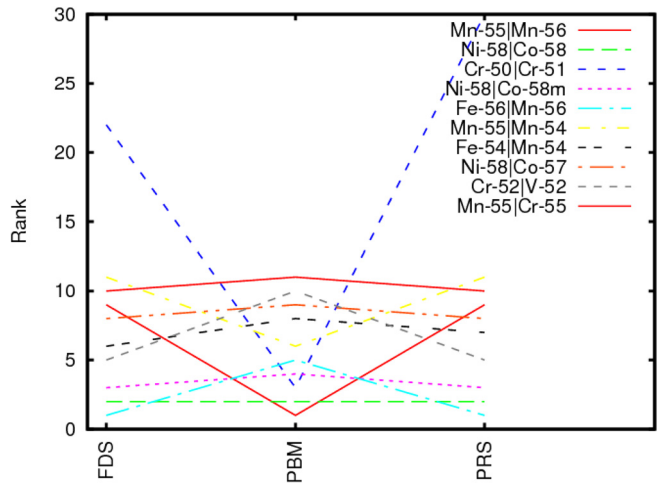

Fig. 2. Comparison of the Alloy test case results, showing the first ten interactions according to the PBM S_{PBM}, ranked accordingly.

sampling, from which it is inferred that round-off effects have become important.

As indicated in Table I, this case involves both an irradiation phase and a cooling period. Care is required in comparing the FDM approach in this instance, for the method uses only the matrix for the cooling phase whereas the other analyses are of the entire history. Although there is still reasonably good correlation between P_{FDS} and P_{PRS}, it is not as good in the other test cases.

III.B.3. Fe

See Table VII and Fig. 6.

III.B.4. LiMix

See Table VIII and Fig. 7. The comparison between the various metrics in Fig. 7 does not at first appear to be

TABLE IV

Alloy+c Case*

Parent	Child	Absolute Pearson		
		40	160	640
Ni-58	Fe-55	0.8132	0.79097	0.79709
Fe-54	Mn-54	0.48716	0.48798	0.48761
Ni-58	Co-57	0.24152	0.23469	0.23442
Mn-55	Mn-54	0.17194	0.16534	0.16563
Ni-60	Co-60*m*	0.16462	0.15008	0.13389
Ni-58	Co-58	0.13754	0.12544	0.11864
Fe-56	Fe-55	9.410×10^{-2}	7.202×10^{-2}	9.237×10^{-2}
Ni-60	Co-60	0.10390	6.218×10^{-2}	5.669×10^{-2}
Ni-58	Co-58*m*	6.996×10^{-2}	5.098×10^{-2}	4.101×10^{-2}
Ti-46	Sc-46*m*	3.614×10^{-2}	1.570×10^{-3}	1.575×10^{-2}
Ti-47	Sc-46	2.538×10^{-2}	2.806×10^{-3}	1.209×10^{-2}
V-49	Sc-46	4.678×10^{-3}	1.198×10^{-2}	1.144×10^{-2}
Co-60*m*	Co-60	1.923×10^{-2}	9.042×10^{-3}	8.303×10^{-3}
Cr-50	V-50	9.279×10^{-3}	1.598×10^{-2}	8.073×10^{-3}
Ni-60	Co-59	1.648×10^{-2}	1.167×10^{-2}	7.639×10^{-3}
Ni-57	Co-57	1.665×10^{-2}	1.499×10^{-2}	7.389×10^{-3}
Co-57	Co-58	2.483×10^{-3}	1.572×10^{-2}	6.780×10^{-3}
Fe-54	Cr-51	2.407×10^{-2}	2.252×10^{-2}	6.773×10^{-3}
Co-57	Co-58*m*	3.906×10^{-2}	9.176×10^{-3}	6.739×10^{-3}
Ti-47	Ti-46	2.828×10^{-2}	1.220×10^{-2}	5.516×10^{-3}
Co-59	Fe-59	8.709×10^{-3}	1.451×10^{-2}	5.499×10^{-3}
Fe-58	Fe-59	2.626×10^{-2}	1.466×10^{-2}	5.289×10^{-3}
Fe-54	Fe-55	2.698×10^{-2}	7.802×10^{-3}	5.261×10^{-3}
Co-58	Fe-58	2.502×10^{-3}	1.069×10^{-3}	5.199×10^{-3}
Ti-47	Sc-46*m*	4.156×10^{-3}	1.867×10^{-2}	5.039×10^{-3}
Cr-50	Cr-51	1.015×10^{-2}	2.073×10^{-3}	4.815×10^{-3}
Co-59	Co-60	1.789×10^{-2}	1.673×10^{-2}	4.743×10^{-3}
Ni-58	Ni-59	2.777×10^{-3}	1.273×10^{-2}	4.581×10^{-3}
Mn-55	Mn-56	1.473×10^{-2}	3.741×10^{-3}	4.456×10^{-3}
Co-58	Co-59	5.478×10^{-3}	6.033×10^{-4}	4.220×10^{-3}

*Values of absolute Pearson correlation coefficient $|r|$ as Monte Carlo sample size increases with N_x.

TABLE V

Alloy+c Case: Rankings for Different Methods

Parent	Child	Sensitivity		
		FDS	PBM	PRS
Cr-52	Cr-51	11	39	49
Mn-55	Mn-54	6	1	4
Fe-56	Fe-55	9	6	7
Ni-58	Co-57	5	3	3
Ni-58	Ni-57	16	20	42
Ni-58	Co-58	1	7	6
Ni-58	Co-58*m*	2	9	9
Ni-58	Fe-55	4	4	1
Fe-54	Cr-51	8	40	17
Fe-54	Mn-54	3	2	2
Cr-50	Cr-51	13	26	26
Ni-62	Fe-59	12	37	44
Ni-60	Co-60	10	14	8
Ni-60	Co-60*m*	7	11	5
Fe-54	Fe-55	15	5	23
Cr-50	V-49	14	16	35
Fe-58	Fe-59	18	27	22
Fe-54	Mn-53	17	18	30
Ni-60	Co-59	22	28	15
Ni-59	Co-58	21	0	0
Ni-58	Fe-54	31	0	0
Ni-59	Co-58*m*	23	0	0
Co-59	Fe-59	19	42	20
Co-59	Co-58	26	0	0
Fe-56	Mn-55	30	0	0
Co-59	Co-58*m*	25	0	0
Ni-59	Fe-55	32	0	0
Ni-62	Ni-63	27	12	33
Fe-55	Mn-54	28	0	0
Co-58	Co-57	24	30	34
Co-57	Co-56	29	44	37
Co-58	Mn-54	33	0	0
Co-58	Co-58*m*	20	62	0

as successful as in the other cases. However, the dominant interaction from the PBM involves tritium for which uncertainty data are not accessible in the database; hence, the FDS and PRS cannot assign it a ranking, and it is omitted from the plot. Moreover, all FDS rankings over 21 similarly correspond to zero uncertainty, and allowing for this, the comparison is as good as any reported herein.

III.B.5. WMix

See Tables IX, X, and XI and Figs. 8, 9, and 10. Table IX suggests that once the Pearson correlation becomes below 0.1, it becomes inaccurate. Figure 8 shows that the lower rankings in terms of sensitivity vary erratically with sampling for similar reasons to do with round-off effects.

TABLE VI

Alloy+c Case: Rankings for Different Methods, Reordered by PBM Ranking

Parent	Child	Sensitivity		
		FDS	PBM	PRS
Mn-55	Mn-54	6	1	4
Fe-54	Mn-54	3	2	2
Ni-58	Co-57	5	3	3
Ni-58	Fe-55	4	4	1
Fe-54	Fe-55	15	5	23
Fe-56	Fe-55	9	6	7
Ni-58	Co-58	1	7	6
Co-60*m*	Co-60	0	8	13
Ni-58	Co-58*m*	2	9	9
Co-58*m*	Co-58	0	10	32
Ni-60	Co-60*m*	7	11	5
Ni-62	Ni-63	27	12	33
Co-58	Co-59	0	13	31
Ni-60	Co-60	10	14	8
Co-59	Co-60*m*	0	15	43
Cr-50	V-49	14	16	35
Co-59	Co-60	0	17	27
Fe-54	Mn-53	17	18	30
Mn-53	Mn-54	0	19	46
Ni-57	Co-57	0	21	16
Ni-58	Ni-57	16	20	42
Mn-55	Mn-56	0	23	29
Mn-56	Fe-56	0	22	0
Co-58*m*	Co-59	0	24	36
Co-57	Co-58	0	25	18
Cr-50	Cr-51	13	26	26
Fe-58	Fe-59	18	27	22
Ni-60	Co-59	22	28	15
Ni-64	Ni-63	0	29	39
Co-58	Co-57	24	30	34

III.B.6. Y203

See Table XII and Fig. 11. The activity at the end of this test case is dominated (99.6%) by two nuclides: N-16 and Y-89*m*; hence, all the detailed rankings by Pearson apart from the first two are suspect. It follows that although the correlation between the two methods appears poor, it is surprisingly good. The reactions O-16| N-16 and Sr-89| Y-89*m* have no corresponding uncertainty estimate, leading to their very high ranking values based on S_{FDS}.

IV. CONCLUSIONS

The sensitivity of the total activity of an inventory to uncertainties in the nuclear data for neutron-induced reactions has been studied. Six different test cases covering

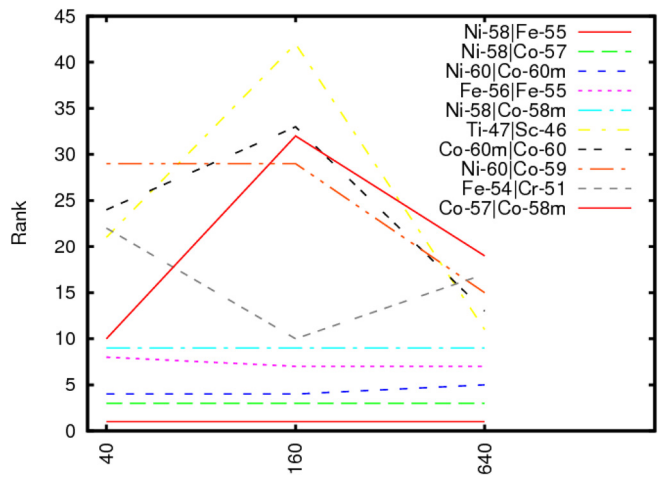

Fig. 3. Comparison of the Alloy+c test case results, showing the first ten odd-numbered interactions according to the scaled Pearson technique value S_{PRS}, for a Monte Carlo sample size of $N_x = 640$ per reaction, as N_x is increased.

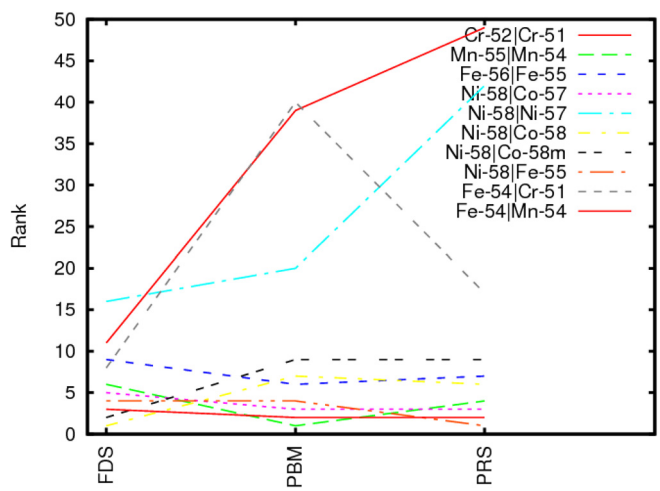

Fig. 4. Comparison of the Alloy+c test case results, showing the first ten interactions by magnitude of the Fréchet derivative. The labels are ordered according to the Fréchet derivative size, so that the top interaction is the most sensitive.

nearly the whole range of atomic masses were considered using three different ranking techniques. It is expected that similar results would be obtained for other inventory properties and other particle species.

The principal result is that a simple PBM gives a sensitivity ranking of interactions that is comparable to rankings based on more conventional measures obtained either by the DM or in terms of Pearson correlation coefficients. Moreover, the PBM is superior in the following ways:

1. It is quick to calculate once the principal pathways have been identified.

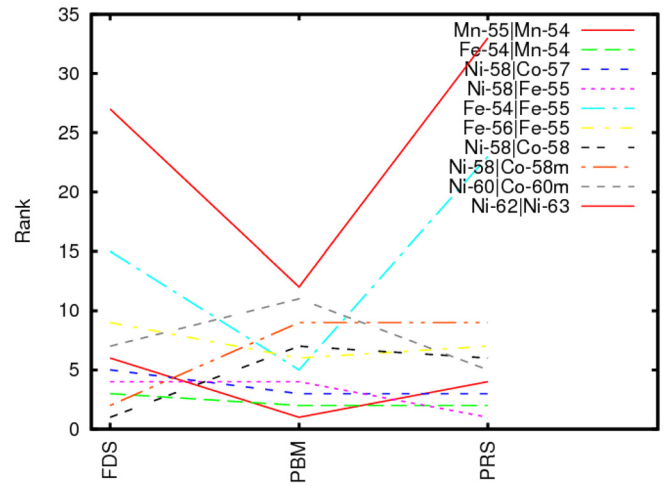

Fig. 5. Comparison of the Alloy+c test case results, showing the first ten interactions according to the PBM S_{PBM} for which comparison is possible.

TABLE VII

Fe Case: Rankings for Different Methods

Parent	Child	Sensitivity		
		FDS	PBM	PRS
Fe-56	Mn-56	1	1	1
Fe-56	Fe-55	4	4	3
Fe-54	Cr-51	3	5	4
Fe-54	Mn-54	2	2	2
Fe-57	Mn-56	13	0	0
Fe-57	Mn-57	5	7	6
Fe-54	Fe-55	6	3	27
Fe-56	Mn-55	7	27	18
Fe-58	Fe-59	9	6	25
Fe-58	Cr-55	10	19	8
Fe-58	Mn-58*m*	11	21	19
Fe-58	Mn-58	12	22	22
Fe-54	Mn-53	8	9	7
Fe-56	Fe-57	16	10	11
Fe-55	Mn-54	14	0	0
Cr-54	Cr-55	20	15	12
Cr-54	V-54	21	26	5
Mn-55	Cr-55	18	24	26
Mn-55	V-52	22	25	16
Mn-55	Mn-56	15	0	0
Fe-57	Fe-58	25	13	24
Mn-55	Mn-54	24	0	0
Fe-57	Cr-54	27	28	14
V-51	V-52	32	16	23
Mn-53	Mn-54	19	8	10
Fe-57	Fe-56	23	0	0
Co-59	Co-60*m*	30	12	21
Co-59	Mn-56	31	0	0
Co-59	Fe-59	28	0	0
Fe-55	Mn-55	17	23	17

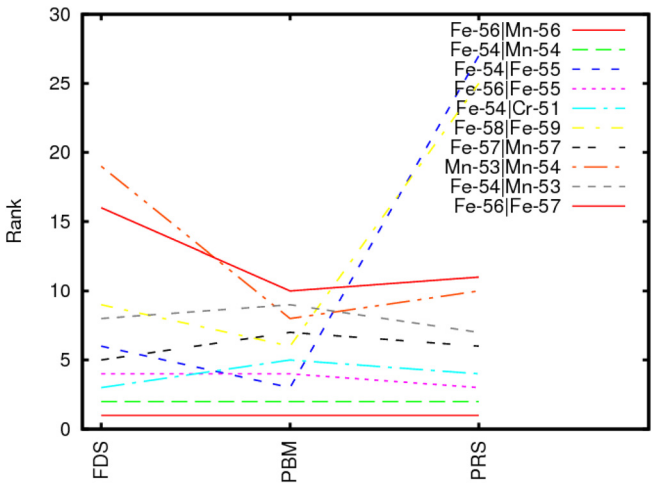

Fig. 6. Comparison of the Fe test case results, showing the first ten interactions according to the PBM S_{PBM}, ranked accordingly.

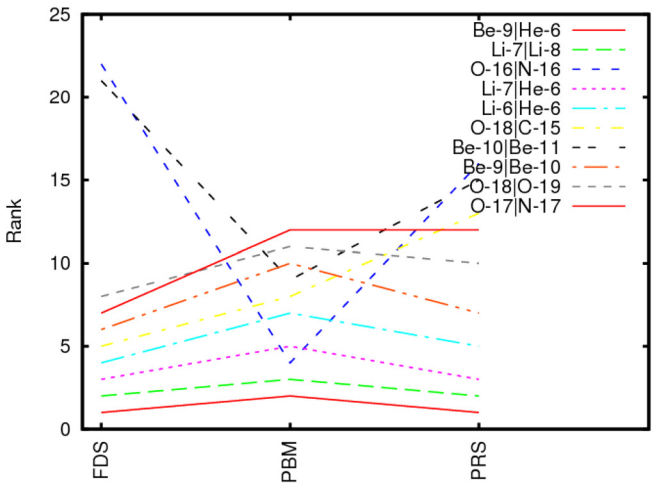

Fig. 7. Comparison of the LiMix test case results, showing the first ten interactions according to the PBM S_{PBM} for which comparison is possible.

2. It does not suffer from numerical difficulties such as underflow (Fréchet direct) or round-off (Pearson) in its evaluation.

3. It may be generalized to the case of multiple irradiation periods just like the pathways-reduced approach itself, whereas the other two techniques require further investigation.

4. It does not require error estimates for every interaction coefficient like Pearson.

An additional noteworthy feature is that the PBM, which is a global measure of uncertainty, is *comparable* with more local measures, provided these others are scaled by the uncertainty in the reaction cross section. This scaling is to be expected since the uncertainty estimates computed by FISPACT-II (Ref. 1, Sec. A.13] involve a multiplication by a measure of cross-section uncertainty (root-mean-square is used to combine reaction coefficients rather than the simple percentages). However, the product also involves the number of child nuclides in the inventory, which is a significantly different measure from the point sensitivity measures.

TABLE VIII

LiMix Case: Rankings for Different Methods

Parent	Child	Sensitivity		
		FDS	PBM	PRS
Li-7	He-6	3	5	3
Li-7	Li-8	2	3	2
Be-9	He-6	1	2	1
O-16	N-16	22	4	16
Li-6	He-6	4	7	5
Li-7	Li-6	24	0	0
Be-9	Be-10	6	10	7
O-18	O-19	8	11	10
O-18	C-15	5	8	13
O-17	N-16	15	0	0
O-17	N-17	7	12	12
O-16	N-15	18	14	11
Be-9	Li-7	11	0	0
He-3	H-3	25	0	0
Be-10	He-6	27	0	0
Be-10	Be-11	21	9	15
O-16	O-17	14	18	4
Li-6	Li-7	13	0	0
N-15	N-16	19	0	0
N-15	C-15	12	0	0
N-15	B-12	9	13	6
C-13	Be-10	10	16	8
O-16	C-13	23	15	17
C-13	Be-9	26	0	0
O-17	O-18	20	0	0
O-17	N-15	17	20	9
O-17	O-16	16	0	0

The value of studying a wide range of test cases is that it demonstrates the general applicability of the above conclusions. In conjunction with modifications to FISPACT-II for more efficient pathways-based analysis in the presence of multiple irradiations, the PBM should be extended to account for loops in the pathways and ultimately integrated into a production version of the FISPACT-II package.

APPENDIX

FRÉCHET DERIVATIVES

As explained in Sec. I, the Bateman equation Eq. (1),

$$\frac{dX}{dt} = \mathsf{A}X, \quad X(0) = X_0, \quad t \in [0, t_f] \ ,$$

TABLE IX

WMix Case*

Parent	Child	Absolute Pearson		
		40	160	640
Re-187	Re-188	0.93702	0.94033	0.94091
Ir-193	Ir-194	0.24971	0.23407	0.24135
Ir-191	Ir-192	0.13306	0.13520	0.13542
Ir-193	Ir-193*m*	0.11155	0.11969	0.11550
Re-185	Re-186	0.10156	8.413×10^{-2}	7.955×10^{-2}
W-184	W-185	6.398×10^{-2}	9.215×10^{-2}	7.856×10^{-2}
W-186	W-187	5.029×10^{-2}	6.135×10^{-2}	6.423×10^{-2}
Re-187	Re-188*m*	2.181×10^{-2}	5.108×10^{-2}	5.264×10^{-2}
Pt-192	Pt-191	4.270×10^{-2}	4.238×10^{-2}	3.215×10^{-2}
Ir-193m	Ir-193	2.090×10^{-2}	9.212×10^{-2}	2.514×10^{-2}
Ir-191	Ir-192*m*	3.290×10^{-2}	1.785×10^{-2}	2.510×10^{-2}
W-186	W-185*m*	4.033×10^{-2}	4.676×10^{-2}	2.323×10^{-2}
Re-187	Re-186	3.941×10^{-2}	2.248×10^{-2}	1.720×10^{-2}
Bi-209	Bi-210	6.132×10^{-2}	1.141×10^{-2}	1.679×10^{-2}
Ir-192	Ir-193*m*	1.539×10^{-2}	1.425×10^{-2}	1.637×10^{-2}
Ir-192	Ir-193	1.845×10^{-2}	1.529×10^{-2}	1.352×10^{-2}
W-182	W-181	1.497×10^{-2}	1.685×10^{-2}	1.274×10^{-2}
Ir-191	Ir-190	2.775×10^{-2}	8.743×10^{-2}	1.263×10^{-2}
Pb-208	Pb-207*m*	3.345×10^{-2}	9.360×10^{-2}	1.217×10^{-2}
Ir-191	Ir-191*m*	2.715×10^{-2}	1.390×10^{-2}	1.167×10^{-2}
Pt-194	Pt-193*m*	1.482×10^{-2}	1.138×10^{-2}	1.020×10^{-2}
W-186	W-185	3.379×10^{-2}	1.427×10^{-2}	9.663×10^{-2}
W-183	W-183*m*	2.160×10^{-2}	1.927×10^{-2}	9.005×10^{-2}
W-183	W-184	5.385×10^{-2}	1.532×10^{-2}	8.812×10^{-2}
Ir-193	Ir-192	2.121×10^{-2}	8.499×10^{-2}	8.497×10^{-2}
Re-185	Re-184*m*	1.874×10^{-2}	7.629×10^{-2}	8.497×10^{-2}
Ir-194	Ir-195*m*	4.688×10^{-2}	5.884×10^{-2}	8.447×10^{-2}
Ir-193	Os-193	3.587×10^{-2}	2.355×10^{-2}	8.253×10^{-2}
Re-188*m*	Re-188	1.010×10^{-2}	4.477×10^{-2}	7.839×10^{-2}
Bi-210*m*	Bi-210	1.836×10^{-2}	3.068×10^{-2}	7.527×10^{-2}

*Values of absolute Pearson correlation coefficient $|r|$ as Monte Carlo sample size increases with N_x.

where $X \in \mathbb{R}^n$ is a vector of nuclide numbers and $\mathsf{A} \in \mathbb{R}^{n \times n}$ is a matrix of nuclear interaction coefficients, controls the evolution of the nuclear activation over time. In this appendix, we focus on the case where A is constant in time.

We are interested in the sensitivity of the total activity Eq. (2),

$$Q = \sum_{k=1}^{n} \lambda_k X_k(t_f) \ ,$$

to the elements in A, which is determined by the n^2 numbers $\partial Q / \partial A_{ij}$. To determine these quantities, we use the matrix exponential and its Fréchet derivative. The matrix exponential of $\mathsf{A} \in \mathbb{R}^{n \times n}$ is defined by

$$e^{\mathsf{A}} = \sum_{k=1}^{\infty} \frac{\mathsf{A}^k}{k!} \ .$$

The Fréchet derivative of the exponential at A in the direction $\mathsf{E} \in \mathbb{R}^{n \times n}$ is denoted by $L_{\exp}(\mathsf{A}, \mathsf{E}) \in \mathbb{R}^{n \times n}$ and satisfies

$$e^{\mathsf{A}+\mathsf{E}} = e^{\mathsf{A}} + L_{\exp}(\mathsf{A}, \mathsf{E}) + o(\|\mathsf{E}\|) \ .$$

For further details of the Fréchet derivative, see Ref. 15, Chap. 3.

The solution to the Bateman equation is given by

$$X(t) = e^{\mathsf{A}t} X_0 \ ,$$

and so,

$$Q = f^T X(t_f) = f^T e^{\mathsf{A}t_f} X_0, \qquad f = [\lambda_1 \ldots \lambda_n]^T \ .$$

Let E_{ij} be the $n \times n$ matrix with a 1 in the (i, j) entry and zeros elsewhere. Now,

TABLE X

WMix Case: Rankings for Different Methods

Parent	Child	Sensitivity		
		FDS	PBM	PRS
Bi-209	Bi-210	14	38	14
Re-187	W-185*m*	29	0	0
Re-187	Re-188*m*	6	12	8
Ir-193	Os-191	35	0	0
Ir-193	Os-191*m*	37	0	0
Bi-209	Pb-207*m*	28	0	0
Ir-193	Ir-192*m*	11	0	0
Re-187	W-185	31	0	0
W-184	W-185*m*	17	50	51
Re-187	W-187	19	0	0
Ir-193	Ir-193*m*	3	16	4
Re-187	Ta-183	32	0	0
W-186	W-185*m*	7	27	12
Re-187	Re-186	8	18	13
Re-187	Re-188	1	4	1
Pt-194	Os-191	26	0	0
Pt-194	Os-191*m*	30	0	0
Pb-208	Pb-207*m*	12	26	19
Re-185	W-185*m*	20	0	0
Ir-193	Ir-192	9	20	26
W-184	W-185	4	13	6
Ir-193	Ir-194	2	1	2
Pt-194	Ir-193*m*	34	0	0
W-186	W-185	10	21	22
W-184	Ta-183	33	0	0
W-184	Ta-182*m*	38	0	0
W-184	Ta-182	36	0	0
W-184	W-183*m*	15	35	55
Pt-194	Ir-194	24	0	0
Pt-194	Pt-193*m*	13	24	21

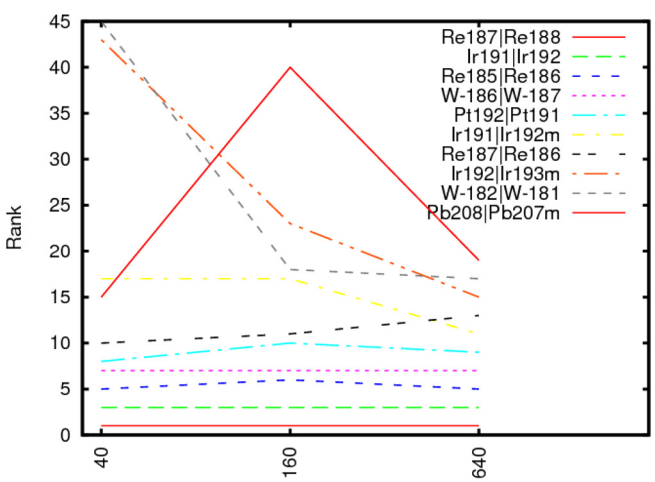

Fig. 8. Comparison of the WMix test case results, showing the first ten odd-numbered interactions according to the scaled Pearson technique value S_{PRS}, for a Monte Carlo sample size of $N_x = 640$ per reaction, as N_x is increased.

TABLE XI

WMix Case: Rankings for Different Methods, Reordered by PBM Ranking

Parent	Child	Sensitivity		
		FDS	PBM	PRS
Ir-193	Ir-194	2	1	2
Re-185	Re-186	0	2	5
Ir-191	Ir-192*m*	0	3	11
Re-187	Re-188	1	4	1
Ir-191	Ir-192	0	5	3
Ir-192*m*	Ir-192	0	6	71
Ir-192	Ir-193*m*	0	7	15
W-186	W-187	5	8	7
Ir-193*m*	Ir-193	0	9	10
Ir-192	Ir-193	0	10	16
W-187	Re-187	0	11	0
Re-187	Re-188*m*	6	12	8
W-184	W-185	4	13	6
Re-186	W-186	0	14	37
Re-188*m*	Re-188	0	15	29
Ir-193	Ir-193*m*	3	16	4
W-185	Re-185	0	17	0
Re-187	Re-186	8	18	13
Ir-194	Ir-195	0	19	62
Ir-193	Ir-192	9	20	26
W-186	W-185	10	21	22
W-182	W-181	0	22	17
Pb-207	Pb-207*m*	0	23	54
Pt-194	Pt-193*m*	13	24	21
Ir-194	Pt-194	0	25	0
Pb-208	Pb-207*m*	12	26	19
W-186	W-185*m*	7	27	12
Ir-191	Ir-191*m*	0	28	20
Re-186	Os-186	0	29	0
Os-186	Os-185	0	30	38

$$
\begin{aligned}
\frac{\partial Q}{\partial A_{ij}} &= \lim_{\delta\to 0} \frac{Q(A_{ij}+\delta) - Q(A_{ij})}{\delta} \\
&= \lim_{\delta\to 0} \frac{f^T(e^{(\mathsf{A}+\mathsf{E}_{ij}\delta)t_f} - e^{\mathsf{A}t_f})X_0}{\delta} \\
&= \lim_{\delta\to 0} \frac{f^T(L_{\exp}(\mathsf{A}t_f, \mathsf{E}_{ij}t_f\delta) + o(\delta))X_0}{\delta} \\
&= t_f f^T L_{\exp}(\mathsf{A}t_f, \mathsf{E}_{ij})X_0 ,
\end{aligned}
$$

where we have used the fact that $L_{\exp}$ is linear in its second argument.

To determine the k largest of these derivatives, we can simply compute them all and sort them. For this, we can use the relationship [Ref. 15, Eq. (3.16)]

$$
\exp\left(\begin{bmatrix} t\mathsf{A} & \mathsf{E}_{ij} \\ 0 & t\mathsf{A} \end{bmatrix}\right) = \begin{bmatrix} e^{t\mathsf{A}} & L_{\exp}(t\mathsf{A}, \mathsf{E}_{ij}) \\ 0 & e^{t\mathsf{A}} \end{bmatrix} , \qquad (A.1)
$$

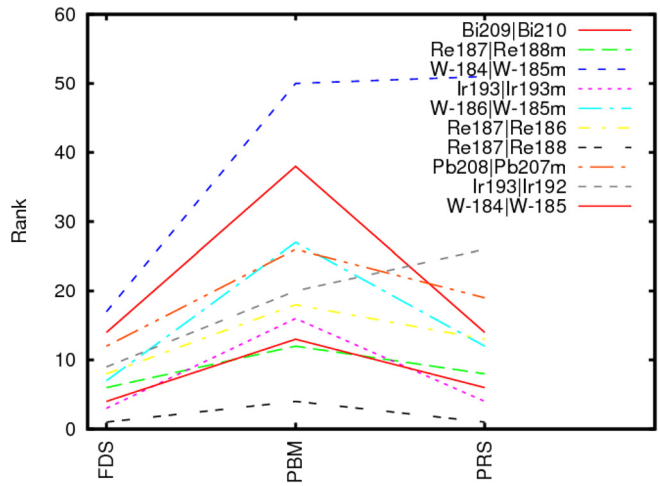

Fig. 9. Comparison of the WMix test case results, showing the first ten interactions by magnitude of the Fréchet derivative. The labels are ordered according to the Fréchet derivative size, so that the top interaction is the most sensitive.

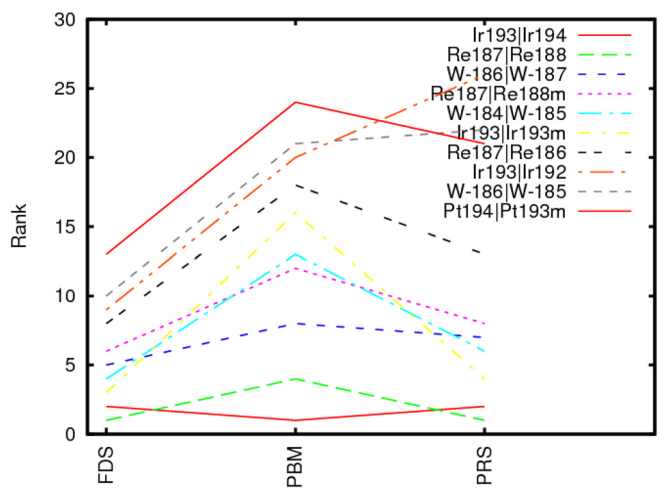

Fig. 10. Comparison of the WMix test case results, showing the first ten interactions according to the PBM S_{PBM} for which comparison is possible.

which yields the formula

$$\exp\left(\begin{bmatrix} t\mathsf{A} & \mathsf{E}_{ij} \\ 0 & t\mathsf{A} \end{bmatrix}\right)\begin{bmatrix} 0 \\ X_0 \end{bmatrix} = \begin{bmatrix} L_{\exp}(t\mathsf{A}, \mathsf{E}_{ij})X_0 \\ e^{t\mathsf{A}}X_0 \end{bmatrix}. \quad \text{(A.2)}$$

Hence, one method to compute $L_{\exp}(\mathsf{A}t_f, \mathsf{E}_{ij})X_0$ is to apply the method from Ref. 16 to compute the product on the left side and then read off the first n components.

However, it is not necessary to carry out n^2 Fréchet derivative evaluations. One suffices, as we now explain. We need some notation. The Kronecker product of two matrices is now textbook for numerical linear algebra; see, e.g., Ref. 17. It is defined for matrices B and C (of any dimension) as the block matrix $\mathsf{B}\otimes\mathsf{C} = (b_{ij}\mathsf{C})$. The vec operator stacks the columns of a matrix one on top of each

TABLE XII

Y2O3 Case: Rankings for Different Methods

Parent	Child	Sensitivity		
		FDS	PBM	PRS
Y-89	Y-90*m*	8	7	11
Y-89	Rb-86*m*	4	3	2
O-16	N-16	30	2	13
Y-89	Rb-86	5	10	5
Y-89	Y-89*m*	2	1	1
Y-89	Y-90	6	8	10
Y-89	Sr-89	3	9	9
Y-89	Y-88	1	5	6
O-18	N-16	11	0	0
O-18	C-15	7	4	3
O-18	N-17	12	11	12
O-17	N-16	9	0	0
O-17	N-17	10	6	7
Y-88	Y-89*m*	13	0	0
O-16	O-17	15	0	0
Sr-89	Y-89*m*	31	0	0
Rb-86	Rb-86*m*	14	0	0
O-18	O-16	21	0	0
Y-90	Y-90*m*	18	0	0
Y-90	Rb-86*m*	23	0	0
O-18	O-17	16	0	0
O-17	O-18	24	0	0
Y-90	Rb-86	22	0	0
Y-90	Y-89*m*	19	0	0
Y-90	Sr-89	20	0	0
O-17	O-16	17	0	0
Y-89*m*	Y-90*m*	28	0	0
Y-89*m*	Rb-86*m*	26	0	0
Y-89*m*	Rb-86	27	0	0
Y-89*m*	Y-90	29	0	0
Y-89*m*	Sr-89	25	0	0

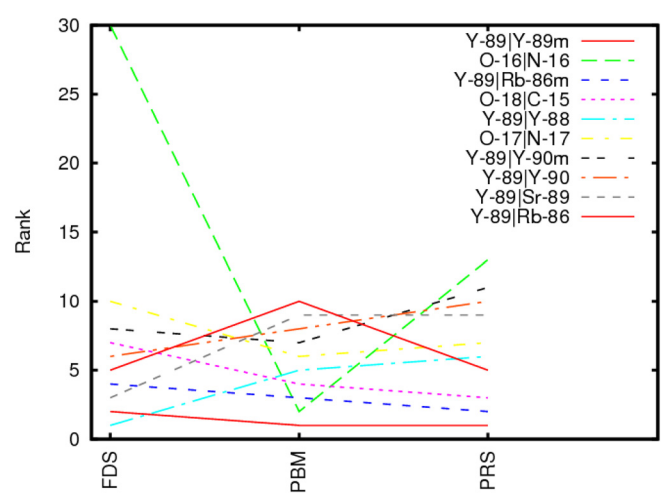

Fig. 11. Comparison of the Y2O3 test case results, showing the first ten interactions according to the PBM S_{PBM}, for which comparison is possible.

other from first to last, producing a long vector. We need the property that $\mathrm{vec}(L_{\exp}(\mathsf{A}, \mathsf{E})) = \mathsf{K}(\mathsf{A})\mathrm{vec}(\mathsf{E})$ for some $n^2 \times n^2$ matrix $\mathsf{K}(\mathsf{A})$ that satisfies $\mathsf{K}(\mathsf{A})^T = \mathsf{K}(\mathsf{A}^T)$. Using the fact that the vec of a scalar is itself and the formula

$$\mathrm{vec}(\mathsf{A}\,\mathsf{X}\,\mathsf{B}) = (\mathsf{B}^T \otimes \mathsf{A})\mathrm{vec}(\mathsf{X}) ,$$

we have

$$\begin{aligned}\frac{\partial Q}{\partial A_{ij}} &= t_f f^{\,T} L_{\exp}(\mathsf{A}t_f, \mathsf{E}_{ij}) X_0 \\ &= \mathrm{vec}(t_f f^T L_{\exp}(\mathsf{A}t_f, \mathsf{E}_{ij}) X_0) \\ &= t_f (X_0 \otimes f)^T \mathrm{vec}(L_{\exp}(\mathsf{A}t_f, \mathsf{E}_{ij})) \\ &\equiv t_f g^T \mathsf{K}(\mathsf{A}t_f)\mathrm{vec}(\mathsf{E}_{ij}) \ ,\end{aligned}$$

where $g = X_0 \otimes f$. Now, since $\mathrm{vec}(\mathsf{E}_{ij})$ is a unit vector, we simply require the k largest elements in modulus of $g^T\mathsf{K}(\mathsf{A}t_f)$, which are the largest k elements in magnitude of $\mathsf{K}(\mathsf{A}t_f)^T g$. We have $\mathsf{K}(\mathsf{A}^T t_f)g = \mathrm{vec}(L_{\exp}(\mathsf{A}^T t_f, \mathsf{E}))$, where $\mathrm{vec}(\mathsf{E}) = g = X_0 \otimes f$, and hence, $\mathsf{E} = f x_0^T$. This means that a single Fréchet derivative evaluation is sufficient, and it can be done using the relationship (A.1) above with an algorithm to compute the matrix exponential such as that in Ref. 18.

The computation of the exponential requires numerous matrix products, which can occasionally cause numerical overflow or underflow due to the large range of magnitudes in the coefficients arising in nuclear activation problems. This may necessitate the use of quadruple precision arithmetic in certain problems. In fact, quadruple precision was used to check the accuracy of all the Fréchet derivatives calculated in the course of the current work.

Acknowledgment

We are grateful to our colleagues J.-C. Sublet and J. W. Eastwood for much advice and assistance. This work has been funded by the Research Councils UK Energy Programme under grant EP/I501045. To obtain further information on the data and models underlying this paper, please contact PublicationsManager@ukaea.uk. The work of Relton and Higham was supported by European Research Council Advanced Grant MATFUN (267526) and Engineering and Physical Sciences Research Council grant EP/I03112X/1.

References

1. J.-C. SUBLET, J. W. EASTWOOD, and J. G. MORGAN, "The FISPACT-II User Manual," CCFE-R(11)11, Issue 6, Culham Centre for Fusion Energy (June 2014).
2. W. ARTER and J. G. MORGAN, "Sensitivity Analysis for Activation Problems," *Proc. Joint Int. Conf. Supercomputing in Nuclear Applications and Monte Carlo (SNA+MC 2013)*, Paris, France, October 27–31, 2013; http://dx.doi.org/10.1051/snamc/201402404.
3. J. W. EASTWOOD and J. G. MORGAN, "Pathways and Uncertainty Prediction in Fispact-II," *Proc. Joint Int. Conf. Supercomputing in Nuclear Applications and Monte Carlo (SNA+MC 2013)*, Paris, France, October 27–31, 2013; http://dx.doi.org/10.1051/snamc/201402403.
4. J. W. EASTWOOD, J. G. MORGAN, and J.-C. SUBLET, "Inventory Uncertainty Quantification Using TENDL Covariance Data in Fispact-II," *Nucl. Data Sheets*, **123**, 84 (2015); http://dx.doi.org/10.1016/j.nds.2014.12.015.
5. J. C. HELTON et al., "Survey of Sampling-Based Methods for Uncertainty and Sensitivity Analysis," *Reliab. Eng. Syst. Saf.*, **91**, *10–11*, 1175 (2006); http://dx.doi.org/10.1016/j.ress.2005.11.017.
6. M. IONESCU-BUJOR and D. G. CACUCI, "A Comparative Review of Sensitivity and Uncertainty Analysis of Large-Scale Systems—I: Deterministic Methods," *Nucl. Sci. Eng.*, **147**, *3*, 189 (2004); http://dx.doi.org/10.13182/NSE03-105CR.
7. D. G. CACUCI and M. IONESCU-BUJOR, "A Comparative Review of Sensitivity and Uncertainty Analysis of Large-Scale Systems—II: Statistical Methods," *Nucl. Sci. Eng.*, **147**, *3*, 204 (2004); http://dx.doi.org/10.13182/04-54CR.
8. B. M. ADAMS et al., "DAKOTA, A Multilevel Parallel Object-Oriented Framework for Design Optimization, Parameter Estimation, Uncertainty Quantification, and Sensitivity Analysis: Version 6.0 User's Manual," SAND2014-4633, Sandia National Laboratories (2014).
9. "SCALE: A Comprehensive Modeling and Simulation Suite for Nuclear Safety Analysis and Design," ORNL/TM-2005/39, Version 6.1, CCC-785, Radiation Safety Information Computational Center, Oak Ridge National Laboratory (June 2011).
10. E. PATELLI et al., "OpenCossan: An Efficient Open Tool for Dealing with Epistemic and Aleatory Uncertainties," *Vulnerability, Uncertainty, and Risk: Quantification, Mitigation, and Management*, pp. 2564–2573, M. BEER, S.-K. AU, and J. W. HALL, Eds., American Society of Civil Engineers (2014).
11. EASY-II European Activation System; http://www.ccfe.ac.uk/EASY.aspx (current as of Feb. 25, 2016).
12. ANSWERS Software Service; http://www.answerssoftwareservice.com (current as of Feb. 25, 2016).
13. A. M. DUNKER, "Efficient Calculation of Sensitivity Coefficients for Complex Atmospheric Models," *Atmos. Environ.*, **15**, *7*, 1155 (1981); http://dx.doi.org/10.1016/0004-6981(81)90305-X.
14. MATLAB, Release 2012a, The MathWorks, Inc., Natick, Massachusetts (2012).

15. N. J. HIGHAM, *Functions of Matrices: Theory and Computation*, Society for Industrial and Applied Mathematics, Philadelphia, Pennsylvania (2008).

16. A. H. AL-MOHY and N. J. HIGHAM, "Computing the Action of the Matrix Exponential, with an Application to Exponential Integrators," *SIAM J. Sci. Comput.*, **33**, *2*, 488 (2011); http://dx.doi.org/10.1137/100788860.

17. G. H. GOLUB and C. F. VAN LOAN, *Matrix Computations*, 4th ed., Johns Hopkins, Baltimore, Maryland (2013).

18. A. H. AL-MOHY and N. J. HIGHAM, "A New Scaling and Squaring Algorithm for the Matrix Exponential," *SIAM J. Matrix Anal. Appl.*, **31**, *3*, 970 (2009); http://dx.doi.org/10.1137/09074721X.